STELLAR ENCOUNTER DRIVEN RED-GIANT STAR MASS LOSS IN GLOBULAR CLUSTERS

Mario Pasquato[1,2], Andrea de Luca[3], Gabriella Raimondo[4], Roberta Carini[5], Anthony Moraghan[1,6],
Chul Chung[1], Enzo Brocato[5], and Young-Wook Lee[1]
[1] Department of Astronomy & Center for Galaxy Evolution Research, Yonsei University, Seoul 120-749, Korea
[2] Yonsei University Observatory, Seoul 120-749, Korea
[3] Laboratoire de Physique Théorique, Ecole Normale Supérieure 24, rue Lhomond, F-75231 Paris Cedex 05, France
[4] INAF-Osservatorio Astronomico di Teramo, Mentore Maggini s.n.c., I-64100 Teramo, Italy
[5] INAF-Osservatorio Astronomico di Roma, Via Frascati 33, I-00040 Monte Porzio Catone, Italy
[6] Academia Sinica Institute of Astronomy and Astrophysics, P.O. Box 23-141, Taipei 106, Taiwan

ABSTRACT

Globular cluster (GC) color–magnitude diagrams (CMDs) are reasonably well understood in terms of standard stellar evolution. However, there are still some open issues, such as fully accounting for the horizontal branch (HB) morphology in terms of chemical and dynamical parameters. Mass loss on the red giant branch (RGB) shapes the mass distribution of the HB stars, and the color distribution in turn. The physical mechanisms driving mass loss are still unclear, as direct observations fail to reveal a clear correlation between mass-loss rate and stellar properties. The HB mass distribution is further complicated by helium-enhanced multiple stellar populations due to differences in the evolving mass along the HB. We present a simple analytical mass-loss model based on tidal stripping through Roche–Lobe overflow during stellar encounters. Our model naturally results in a non-Gaussian mass-loss distribution with high skewness and contains only two free parameters. We fit it to the HB mass distribution of four Galactic GCs, as obtained from fitting the CMD with zero age HB models. The best-fit model accurately reproduces the observed mass distribution. If confirmed on a wider sample of GCs, our results would account for the effects of dynamics in RGB mass-loss processes and provide a physically motivated procedure for synthetic CMDs of GCs. Our physical modeling of mass loss may result in the ability to disentangle the effects of dynamics and helium-enhanced multiple populations on the HB morphology and is instrumental in making HB morphology a probe of the dynamical state of GCs, leading to an improved understanding of their evolution.

Key words: globular clusters: general – globular clusters: individual (NGC 5904, NGC 6093, NGC 6266, NGC 6752) – stars: horizontal-branch – stars: kinematics and dynamics – stars: mass-loss

Online-only material: color figures

1. INTRODUCTION

Globular clusters (GCs) are the environment of choice for testing our theoretical understanding of stellar evolution. Stellar evolution models have generally been able to reproduce the features of GC color–magnitude diagrams (CMDs). Yet some open issues still remain, such as mass loss along the red giant branch (RGB), which in turn influences the later stages of stellar evolution (Lafon & Berruyer 1991; Harper 1996; Origlia et al. 2002, 2007, 2010; Dupree et al. 2009), in particular, the color and temperature distribution of stars along the horizontal branch (HB). This problem is also difficult to decouple from the influence of helium-enhanced multiple stellar populations, which are widespread in GCs and heavily influence HB morphology (see Bedin et al. 2004; Gratton et al. 2004, 2010; Piotto et al. 2005; Bragaglia et al. 2010; Dalessandro et al. 2011, 2013; Monelli et al. 2013). Synthetic CMDs are usually built assuming an arbitrary RGB mass-loss distribution, such as a Gaussian with adjustable variance (Rood 1973; Lee et al. 1994; Brocato et al. 2000; Raimondo et al. 2002). Various mass-loss laws (see Catelan 2009 for a review) have been proposed and implemented in stellar evolution prescriptions (e.g., Renzini & Voli 1981) with Reimers law (Kudritzki & Reimers 1978) remaining the most prominent. However, a full understanding of the underlying physics of wind-driven mass loss is still elusive (e.g., see Dupree et al. 2009; Boyer et al. 2010, and references therein) and direct observations of live mass loss by the detection of warm circumstellar dust as far infrared excess (Groenewegen

2012a, 2012b; Origlia et al. 2007, 2014) are feasible but difficult in crowded GC environments (Boyer et al. 2010; Origlia et al. 2010). It is likely that future ALMA observations may help shed further light on this and related issues (Olofsson 2008; Groenewegen et al. 2009).

A low-mass star would have to lose a few tenths of a solar mass on the RGB in order to be positioned on the hot end of the zero-age HB (ZAHB). Instead, a lower mass loss (i.e., of the order of a few hundredths of a solar mass) is required to produce cool ZAHB stars. There is evidence that mass loss may be due to distinct physical processes which occur in order to populate different temperature ranges on the HB (see, e.g., Ferraro et al. 1998). Moreover, mass loss may take place in relatively brief events and may be weakly dependent on stellar properties (Origlia et al. 2002, 2007; McDonald et al. 2009), as would be expected if the mass-loss mechanisms were not fully intrinsic to the star but partly due to, or triggered by, external factors. Stellar distributions and peculiarities in HB morphology, such as gaps, and subluminous stars bluer than the canonical end of the HB, the so-called blue hook observed in the UV CMDs of the most massive GCs (D'Cruz et al. 1996; Piotto et al. 1999; Whitney et al. 1998; Brown et al. 2001, 2010; Busso et al. 2007; Dalessandro et al. 2008a, 2008b), may be important clues for the study of HB star formation mechanisms. In particular, the formation of extremely hot HB objects ($T_{\rm eff} \geqslant 32{,}000$ K) cannot be explained by the canonical stellar evolution and mass-loss theories. Interestingly, they were proposed to be the progeny of stars that, due to an unusually large mass loss, left the RGB

before the helium flash and ignited helium later on during the white dwarf (WD) cooling sequence (Castellani & Castellani 1993; D'Cruz et al. 1996; Brown et al. 2001). Alternatively, they may also be the progeny of the helium-enriched main-sequence (MS) population, as proposed in the case of ω-*Cen* and NGC 2808 (e.g., Lee et al. 2005).

In this paper, we present a simple analytical model of the effects of stellar encounters on RGB mass loss, and use this model to predict the HB mass distributions obtained from samples of HB stars in the Galactic GCs NGC 5904, NGC 6093, NGC 6266, and NGC 6752. These clusters all show an extended HB (EHB) morphology (Lee et al. 2007), the presence of exotica likely originating from stellar interactions (see, e.g., Anderson et al. 1997; Beccari et al. 2006), and an intermediate-to-old dynamical age, which may be an indication of dynamical effects playing a role in the RGB mass-loss mechanism (Pasquato et al. 2013). In these environments, our mass-loss law provides a remarkably good fit to HB-mass data, suggesting that tidal stripping through stellar encounters is probably the principal mechanism mediating the effect of dynamics on mass loss. A related issue is that of red-giant (RG) collisions and collisional depletion in dense clusters, as discussed, e.g., by Portegies Zwart (1996), Shara et al. (1998), and Adams et al. (2004). We are also currently running smoothed particle hydrodynamics (SPH) simulations of stellar collisions to produce a more detailed model that we will compare to a much larger database of HB mass distributions (A. Moraghan et al., in preparation).

Our approach differs from previous studies (e.g., Buonanno et al. 1997; Recio-Blanco et al. 2006; Pasquato et al. 2013), which mainly looked for correlations between a collisional parameter and a cluster's HB morphology indicator, because it focuses on the shape of the mass-loss distribution of HB stars. The shape of the mass-loss distribution, as measured, e.g., by the skewness parameter, is independent of the typical amount of mass loss (as measured by the mean or median mass loss) and of the dispersion in mass loss (as measured by the standard deviation or other suitable estimators of dispersion). Thus, we test a qualitatively different point with respect to previous studies, potentially complementing them (see also the discussion in Dotter 2013, who elaborates on this point from a slightly different perspective).

2. PRELIMINARY ORDER OF MAGNITUDE ESTIMATE

Before dealing with the full calculation, let us quickly estimate the fraction of RGB stars that undergo collisions resulting in significant mass loss in a typical GC. If we call $r_{\rm RGB}$ the radius of the RGB star, then we can assume that encounters within the distance $hr_{\rm RGB}$ produce a significant mass loss, where h is a numerical factor. The cross section for such an encounter will be $\sigma = \pi h^2 r_{\rm RGB}^2$, neglecting both gravitational focusing effects and the radius of non-RGB stars. An RGB star orbiting in a GC core moves with average velocity v during its RGB lifetime $t_{\rm RGB}$. During this time, it will have an encounter if a star is found within the cylindrical volume

$$V = \sigma v t_{\rm RGB} = \pi h^2 r_{\rm RGB}^2 v t_{\rm RGB}, \tag{1}$$

so the probability of having an encounter is given by the number density n times the volume V:

$$P = n \times \pi h^2 r_{\rm RGB}^2 v t_{\rm RGB}. \tag{2}$$

Typical GC-core values are $v = 10$ km s^{-1}, $n = 5 \times 10^5$ pc^{-3}, and for GC RGB stars[7] $t_{\rm RGB} = 100$ Myr and $r_{\rm RGB} = 200 \, R_\odot$, so that

$$P = h^2 \times 3 \times 10^{-2}. \tag{3}$$

Depending on the value of $h \approx 1$–10, the probability ranges from about some percent even up to 100%. It is difficult to constrain the expected probability in this rough approximation, because of the quadratic dependence on the unknown h. However, adopting $h = 2$, Equation (3) yields 12%, which is compatible with the typical fractions of EHB or Blue Hook stars found in GCs with an EHB morphology (Dalessandro et al. 2008a, 2008b, 2011). This is a hint that stellar collisions may play a role in the EHB formation mechanism, but a quantitative treatment is necessary if we want to obtain better constraints.

3. THE MODEL

We consider encounters between a single RGB star and a single cluster member (most likely an MS star). Initially, we neglect gravitational focusing and approximate the orbits of both stars with straight lines, while in the next subsection we include the effects of gravitational focusing derived from a full solution of the two-body problem. It is clear that binary–single and binary–binary collisions (where the RGB or the scattering star, or both, were initially members of a binary) may play an important role in the actual mechanism of encounter-driven mass loss, because of the strong increase of the cross section of the interaction. However, EHB stars in clusters do not appear to be prevalently members of a binary system (Moni Bidin et al. 2006, 2009, 2011). Therefore, considering the daunting complexity of the dynamics of such encounters (see Hills 1975; Heggie & Hut 1993), we decide not to address this issue in the present paper. To be sure, Milone et al. (2012) find a loose anticorrelation between the maximum HB temperature and MS binary fraction (as determined photometrically), so the issue is surely worthy of consideration and will be explored in detail in a follow-up paper.

3.1. Negligible Gravitational Focusing Approximation

We consider the impact parameter during a collision

$$b = |\boldsymbol{x} - (\boldsymbol{x} \cdot \hat{v}) \, \hat{v}|, \tag{4}$$

where $\boldsymbol{x}$ and $\boldsymbol{v}$ are the scatterer star's position and velocity, and we assume that an encounter with impact parameter b causes mass loss when an RGB star overflows the associated Hill radius:

$$r_H = k \left(\frac{m_i}{M_{\rm RGB}} \right)^{1/3} b, \tag{5}$$

where $k \approx 1$ is a numeric factor and $m_i/M_{\rm RGB}$ is the mass ratio of the impactor to the RGB star. We approximate the density ρ of the external layers of the RGB star as a power law in radius r with the expression

$$\rho(r) \propto r^{-11/3}. \tag{6}$$

By integrating over the RGB star volume from r_H to the surface, the overflowing mass we obtain is

---

[7] The size of RGB stars varies over time during their evolution before reaching the RGB-tip value, so the following is an overestimate. A more accurate calculation would involve integrating the cross section for collisions over the RGB lifetime of a relevant stellar model.

$$\delta M = \int_{r_H}^{r_{RGB}} 4\pi r^2 \rho(r)dr = A\left[1 - \left(\frac{b}{a}\right)^{2/3}\right], \quad (7)$$

where A represents the maximum amount of mass that can be lost in the event of a head-on collision, and

$$a = \frac{r_{RGB}}{k}\left(\frac{M_{RGB}}{m_i}\right)^{1/3} \quad (8)$$

is the maximum impact parameter for which mass loss may take place. In the notation of Section 2, we can write

$$h = \frac{1}{k}\left(\frac{M_{RGB}}{m_i}\right)^{1/3} \gtrsim 1. \quad (9)$$

Since Equation (6) holds only in the external layers, in general, $A \neq M$, so we allow for it to be a free parameter. We also introduce a zero-point correction parameter B, possibly related to systematic uncertainties in the determination of the RGB star mass before the encounter. Therefore, Equation (7) becomes

$$\delta M = A\left[1 - \left(\frac{b}{a}\right)^{2/3}\right] + B. \quad (10)$$

We model the phase-space distribution of stars in a GC as isotropic and with constant density. We will consider the impact parameter distribution $f(b)$ within a sphere of radius a, i.e., under the condition that $b < a$ and the assumption that stars with $b < a$ uniformly populate the $r < a$ sphere. The resulting impact parameter distribution is expressed as

$$f(b) = \frac{3b\sqrt{1 - \frac{b^2}{a^2}}}{a^2}. \quad (11)$$

This is a zeroth-order approximation, given that the number density of stars in the cluster actually varies by orders of magnitude when moving along an eccentric stellar orbit that dips into the GC core and reaches to the outskirts over a timescale that is potentially shorter than RGB lifetime. However, the assumption that underlies our result is increasingly accurate for decreasing b (i.e., increasing mass loss), so we expect environmental factors to affect the low-mass-loss part of our distribution more than its high-mass-loss tail. Note that at small $b \ll a$, $f(b)$ is simply linear. Indeed, the parameter a can be seen as a regularizer of the distribution for large b and at small b one recovers $f(b)\,db \propto 2\pi b\,db$. It is also useful to consider the cumulative distribution function $F(b)$, defined as the probability of having an impact parameter smaller than b. We obtain

$$F(b) = 1 - \left(1 - \frac{b^2}{a^2}\right)^{3/2}, \quad (12)$$

and then for $b \ll a$ the expected quadratic behavior is recovered, $F(b) \propto b^2/a^2$.

Finally, combining Equation (11) with Equation (10), we obtain the probability distribution of δM as[8]

---

[8] Given the theoretical distribution of impact parameters in Equation (11) and the relation to mass loss assumed in Equation (10), there are several ways to obtain Equation (13). For example, we can note that Equation (10) is monotonic so that impact parameters larger than a given value b correspond to mass loss smaller than $\delta M(b)$. In this way, the cumulative distribution of δM can be obtained by applying Equation (10) to the cumulative distribution of $1 - b/a$. Afterward, Equation (13) can be obtained by derivation with respect to δM. This procedure is general and applies to any distribution of impact parameters and to any mass-loss law that is monotonic in the impact parameter.
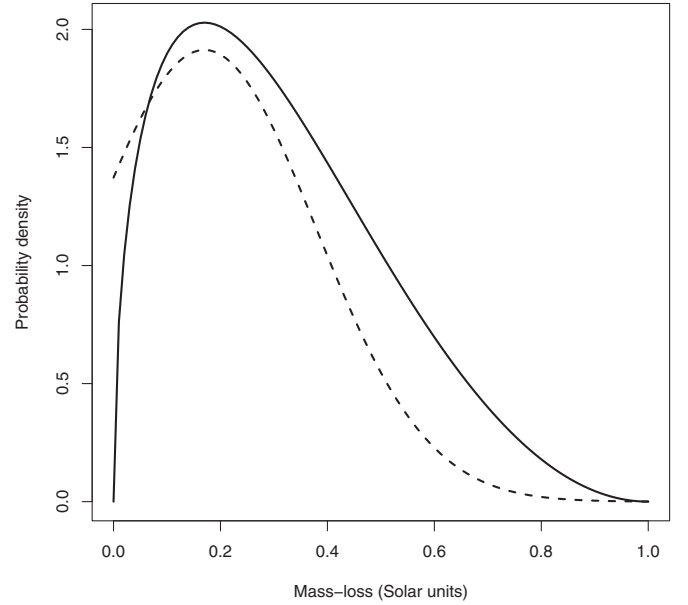

Figure 1. Solid line is the distribution of Equation (13) for $A = 1$ and $B = 0$. The dashed line is a Gaussian with the same FWHM and mode. Note how our model shows a heavy tail toward high mass loss compared to the Gaussian.

$$g(\delta M) = \frac{9}{2A}\left(1 - \frac{\delta M - B}{A}\right)^2 \sqrt{1 - \left[1 - \left(\frac{\delta M - B}{A}\right)\right]^3}. \quad (13)$$

The distribution lacks an adjustable shape parameter: changes in the values of the parameters A and B correspond to a linear rescaling[9] and a rigid translation, respectively, and they do not affect the shape of the curve which is skewed toward high values of mass loss. We show the shape of the distribution for $A = 1$ and $B = 0$ in Figure 1, where a Gaussian distribution with the same FWHM and mode (maximum) is also plotted for comparison. Note how the tail of the Gaussian distribution drops considerably faster for increasing values of mass loss with respect to our model.

Note that Equation (13) describes the distribution of the mass loss only for stars that underwent at least a collision, i.e., an encounter with $b/a < 1$. We also neglect multiple collisions so that at least a collision means exactly one collision.[10] The probability of having a collision does not enter Equation (13), and it is impossible to use it to estimate the maximum impact parameter a resulting in mass loss. The probability P of colliding is irrelevant to the shape of the distribution of mass loss for those stars that actually collided, and vice versa. The full mass-loss distribution, including stars that did not collide, is

$$g_{all}(\delta M) = Pg(\delta M) + (1 - P)\delta_D(\delta M), \quad (14)$$

where δ_D is the Dirac delta function centered in 0. In a real CMD, however, photometric errors, differential reddening, and mass-loss mechanisms not related to encounters would broaden the delta function. To model this, we would need to introduce further parameters, limiting the predictivity of our model and leading to a more complex analysis that is beyond the scope of

---

[9] For the normalization to be preserved, however, A also has to appear in the denominator of Equation (13).

[10] This is inconsistent when $P \to 1$ in Equation (3) because the probability of double (independent) collisions scales as P^2. However, we assume that the cross section is considerably reduced after the first collision, as is the case when most of the envelope mass is stripped.

Table 1
Properties of Our Comparison Clusters

Name	M_V	c	E_{B-V}	$(m-M)_V$	[Fe/H]
NGC 5904 (M5)	−8.81	1.73	0.02	14.46	−1.33 ± 0.02
NGC 6093 (M80)	−8.23	1.68	0.03	15.75	−1.75 ± 0.08
NGC 6266 (M62)	−9.18	1.71c	0.03	15.64	−1.18 ± 0.07
NGC 6752	−7.73	2.50c	0.06	13.15	−1.55 ± 0.01

Notes. Columns: cluster identification; total cluster magnitude in V, central concentration, reddening, and distance modulus from Harris's catalog; [Fe/H] from Carretta et al. (2009).

this paper. In the following, however, we will assume $P = 1$ and neglect the Dirac delta term, even though this is justified only in extremely high-density environments where, for a given $h \approx 2$, the probability of collision P can be inflated by a larger numeric coefficient with respect to that in Equation (3), which refers to average cluster values.

3.2. Full Model with Gravitational Focusing

We now add gravitational focusing to the simple model outlined above. The periastron during an encounter is a function of the impact parameter and relative velocity:

$$r(b, v) = \frac{2Gm\left(\sqrt{\frac{b^2 v^4}{4G^2 m^2} + 1} - 1\right)}{v^2}, \qquad (15)$$

where $m = m_i + M_{\mathrm{RGB}}$ is the sum of the two star's masses, and consistency with the previous section is ensured given that $r(b, v) \xrightarrow{v \to \infty} b$. The distribution of the impact parameter is, as before, given by Equation (11), but now we assume that the relevant parameter for mass loss is the periastron. Therefore the mass lost is now a function of the periastron, i.e.,

$$\delta M(r) = A\left[1 - \left(\frac{r}{r_a}\right)^{2/3}\right] + B, \qquad (16)$$

where the maximum radius at which we have mass lost is $r_a \equiv r(a)$. The distribution of r can be obtained by combining Equations (15) and (11),

$$P(r) = \frac{3(2\nu\rho + 1)\sqrt{\nu - \nu\rho^2 - \rho}}{2a\nu^{3/2}}, \qquad (17)$$

while its cumulative distribution, defined as the probability of having a periastron smaller than r, takes the form

$$C(r) = 1 - \left(1 - \frac{\rho(\nu\rho + 1)}{\nu}\right)^{3/2}, \qquad (18)$$

where we set $\rho = r/a$ and

$$\nu = \frac{av^2}{4Gm}. \qquad (19)$$

The dimensionless quantity ν is key to the following discussion, in that it parameterizes the strength of gravitational focusing. It is proportional to the ratio between the typical velocity of stars v and a scale escape velocity from the RGB star (the scale being set by a, the maximum impact parameter for which mass loss occurs, which is a free parameter in our model), squared.

Table 2
Relevant Dynamical Properties and Maximum HB Temperature of Our Comparison Clusters

Name	σ_K	Γ_{coll}	ν	f_b	$\log T_{\mathrm{HB}}^{\mathrm{max}}$
NGC 5904 (M5)	9.01	−14.30	1.0	0.022 ± 0.006	4.176
NGC 6093 (M80)	10.37	−13.68	1.3	0.012 ± 0.006	4.477
NGC 6266 (M62)	16.57	−14.22	3.4	NA	4.477
NGC 6752	NA	NA	NA	0.010 ± 0.006	NA

Notes. Columns: cluster identification; velocity dispersion from King model fit from McLaughlin & van der Marel (2005); collisional parameter from Table 1 of Recio-Blanco et al. (2006); gravitational focusing parameter ν as defined in Equation (19), normalized to NGC 5904; total MS binary fraction ($f_{\mathrm{bin}}^{\mathrm{TOT}}$ in WFC field) from Table 2 of Milone et al. (2012); and maximum HB temperature.

The condition $\nu > 1/2$ holds for hyperbolic orbits. Typical values in GC cores are of the order of one for a which is of the order of several times the RGB radius. Clearly $P(r) \to f(r)$ for $\nu \gg 1$, and gravitational focusing becomes negligible in this limit, recovering our previous results. On the other hand, if the gravitational focusing is not negligible and ν is finite, then the behavior at small r is strongly modified. In fact, in the relevant region at small periastron, i.e., $\rho \ll \nu$, the cumulative distribution of the periastron becomes linear $C(r) \simeq (3\rho/2\nu)$. This should be compared with the quadratic behavior at small b that we had in Equation (12).

The general distribution of the mass loss, according to Equation (16), is then given by

$$P(\delta M) = \frac{9(u^{3/2}(z-1)+1)\sqrt{u(z+1-2u^{3/2}-u^3(z-1))}}{2A(z+1)^{3/2}}, \qquad (20)$$

where $u = (A + B - M/A)$ and $z = \sqrt{1 + 4\nu^2}$. In Figure 2, we compare the shape of the distribution predicted by Equation (20) for various values of ν with the limit $\nu \to \infty$. The main effect of gravitational focusing is, predictably, to thicken the high-mass-loss tail and to make the distribution somewhat more symmetric, lowering its skewness. The physical interpretation of this occurrence is that gravitational focusing increases the proportion of encounters that remove a large amount of mass in the distribution. However, it is easy to note that even for low values of ν (of the order of unity to several), the skewed shape of the distribution that is distinctive of our result is still readily visible. In the following sections, for simplicity, we limit our quantitative comparison to the data to the $\nu \to \infty$ limit. However, we will see that the cluster most affected by gravitational focusing effects (NGC 5904; see Table 2) deviates the most from the expectations of Equation (13), and precisely in the direction of increased symmetry in the distribution. Meanwhile, NGC 6266, the least affected, shows the best agreement with Equation (13).

4. TESTING THE MODEL ON GLOBULAR CLUSTERS

In order to test our mass-loss law in detail, we consider four GCs, namely, NGC 5904, NGC 6093, NGC 6266, and NGC 6752. See Tables 1 and 2 for a summary of the sample properties. It has become clear in recent years that GCs are not simple stellar populations, but may host chemically distinct subpopulations, typically with an enhanced helium abundance. These helium-rich populations can make up a substantial fraction of all cluster stars, and can play a role in shaping the HB morphology as well (e.g., Gratton et al. 2010). However,
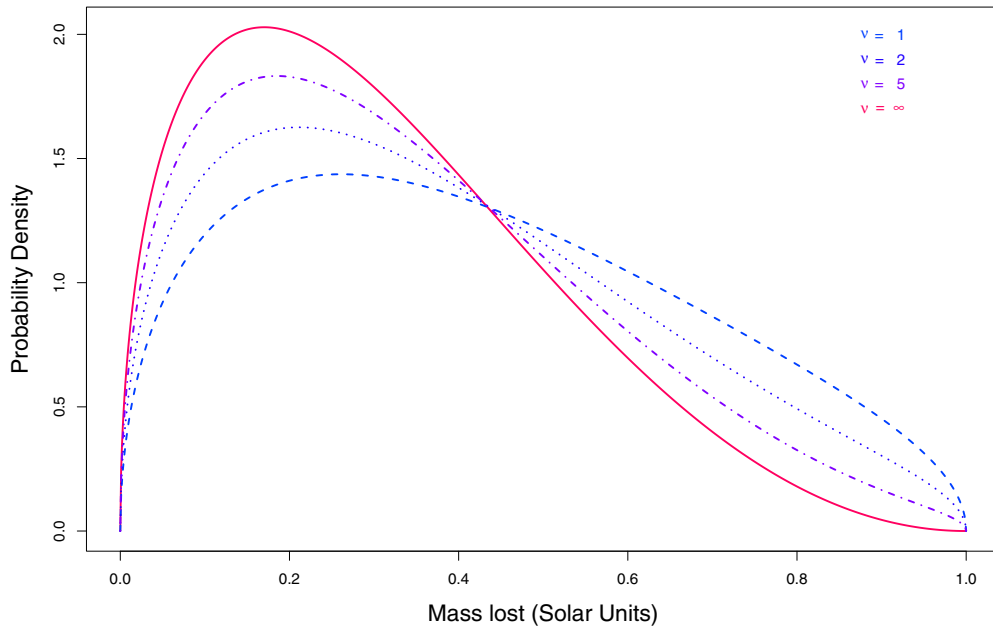
Figure 2. Red solid line is the distribution of Equation (13) for $A = 1$ and $B = 0$, corresponding to the limit of Equation (20) for which gravitational focusing is negligible, i.e., $\nu \to \infty$. The dot-dashed, dotted, and dashed lines in progressively darker shades of purple correspond to lowering values of the dimensionless parameter ν in Equation (20) (see Equation (19) for the definition of ν), i.e., $\nu = 5, 2, 1$, respectively. The shape of the distribution approaches the $\nu \to \infty$ limit already for $\nu = 1$, which is a typical value in GCs if we assume a value of the parameter a in Equation (19) of the order of several times the RGB radius.
(A color version of this figure is available in the online journal.)

it should be clear that in this section, we are exploring the ability of our model to reproduce the HB morphology without including other mechanisms able to modify the distribution of the stars in the HB.

The clusters in our sample are chosen in order to have well or moderately extended blue HB tails. NGC 5904 and NGC 6266 possess a similar metal content, but the latter presents an HB that is more extended toward high temperatures. In NGC 5904, the $c_{U,B,I}$ distribution of RGB stars confirms the multimodality of the RGB (Monelli et al. 2013).

NGC 6093 (M80) is one of the densest GCs in the Milky Way. Apart from GC abundance anomalies, there is no photometric evidence of multiple stellar populations to date, as recently shown by Monelli et al. (2013), who do not find multiple RGB sequences using the $c_{U,B,I}$ color.

NGC 6752 is a moderately metal poor cluster with [Fe/H]~ -1.55 (Yong et al. 2005; Carretta et al. 2010), with large star-to-star variations in O, N, Na, Mg, and Al. The Na–O and Mg–Al anticorrelations have been observed by Yong et al. (2005) and Carretta et al. (2012). Recently, in this cluster, three main populations of stars have been photometrically identified by Monelli et al. (2013).

For each cluster, the starting values of reddening and distance are taken from Harris's catalog[11] (Harris 1996), except for NGC 6093, for which we assumed values from Recio-Blanco et al. (2005). Note that here we neglect a possible broadening of the CMDs due to differential and non-uniform reddening across the cluster. For instance, NGC 6266 is located in the direction of the galactic center and its extinction across its visible surface is nonuniform, causing the features in its CMD to be broadened (Alonso-García et al. 2011).

Observations were taken from the *HST*-WFPC2 database of Piotto et al. (2002),[12] except for NGC 6752 from the *HST*-ACS

data by Sarajedini et al. (2007).[13] We derive the best fit for each cluster by assuming [Fe/H] from the metallicity scale by Carretta et al. (2009); see Table 1. We produce synthetic CMDs from the MS phase up to the asymptotic branch using the stellar population synthesis code SPoT (Stellar POpulation Tools, see for details and ingredients Raimondo et al. 2005; Raimondo 2009). The metallicity values we adopt are $Z = 0.001$ for NGC 5904 and NGC 6266, and $Z = 0.0006$ for NGC 6093 and NGC 6752. As for ages, the best fit is found at an age of 13 Gyr in the case of NGC 6093, and 12 Gyr for NGC 5904 and NGC 6266, which are all in agreement with the relative age scale of Marín-Franch et al. (2009). An age range spanning from 11 Gyr up to 14 Gyr is also taken into account in order to explore the effect of age on the mass at the tip of the RGB. Our model in any case is sensitive to the RGB-tip mass only through the shift-parameter B, while the overall shape of the mass-loss distribution function is the same for different values of the mass at the tip of the RGB.

The ZAHB from the best-fit model is used to derive the mass distribution along the HB by counting stars in 0.01 solar-mass bins along it, as illustrated in the CMD of NGC 6266 in Figure 3. The entire synthetic CMD and mass values are from canonical theoretical stellar evolution models (Pietrinferni et al. 2006 and references therein). This choice is justified by the fact that we are looking at a pure dynamical effect of mass loss on the HB mass distribution. We plan to include the effects of helium-enhancement, age, chemistry, and possibly further parameters in a forthcoming paper, along with refinements of our model.

4.1. Results

We obtained a simple physical model of collision-mediated RGB mass loss. Its main prediction is the asymmetry of the mass-loss probability distribution function, due to the
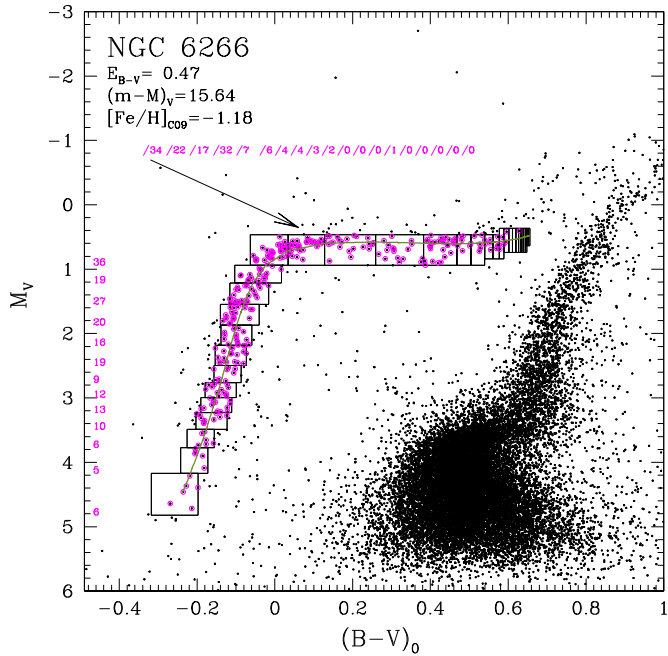

Figure 3. Observed color–magnitude diagram of NGC 6266. The ZAHB location (dark green line) for classical HB evolutionary models of $Z = 0.001$ is shown. The boxes correspond to mass intervals of $\delta M = 0.01 M_\odot$ that we used to derive the histogram of mass distribution along the observed HB.

(A color version of this figure is available in the online journal.)

Table 3
Summary of Our Results on Our Comparison Clusters

Name	N	A	B	S-W	Skew
NGC 5904	284	0.16 ± 0.02	0.158 ± 0.005	7.3×10^{-11}	0.00 ± 0.09
NGC 6093	328	0.24 ± 0.03	0.143 ± 0.009	3.4×10^{-14}	0.17 ± 0.09
NGC 6266	309	0.222 ± 0.007	0.158 ± 0.002	2.8×10^{-4}	0.17 ± 0.08
NGC 6752	120	0.29 ± 0.02	0.166 ± 0.006	7.9×10^{-7}	0.17 ± 0.06

Notes. Fit parameters with associated uncertainties (A, ΔA, B, ΔB), Shapiro–Wilk test p-value (S-W p), and quantile-based skewness parameter (skew). The B coefficients are compatible within 2σ error bars, while the A coefficients are not.

fundamental fact that distant encounters that result in lower mass loss are more frequent than near encounters that produce high mass loss. This is a feature that we expect to be shared by all collision-based models, whatever the details of how the mass-stripping interaction is modeled. Instead, a Gaussian mass-loss distribution is symmetric by construction. In our four clusters, we obtained the mass-loss distribution by subtracting the HB mass from the mass at the tip of the RGB as obtained self-consistently by the best fit to the CMD. We then tested the Gaussianity of the mass-loss distribution thus obtained by using a Shapiro–Wilk (S-W) Gaussianity test (Royston 1982) and found that at different confidence levels (see the p-values listed in Column 5 of Table 3) it can be rejected.

To measure the amount of symmetry observed in the empirical data set independently from the Gaussianity hypothesis, we introduce a robust skewness parameter based on the sample median ($q_{50\%}$) and 25% and 75% quantiles ($q_{25\%}$ and $q_{75\%}$), defined as

$$s = \frac{1}{2} - \frac{q_{50\%} - q_{25\%}}{q_{75\%} - q_{25\%}}, \qquad (21)$$

obtaining the values listed in Column 6 of Table 3. The uncertainty on s is obtained by bootstrap resampling. A value
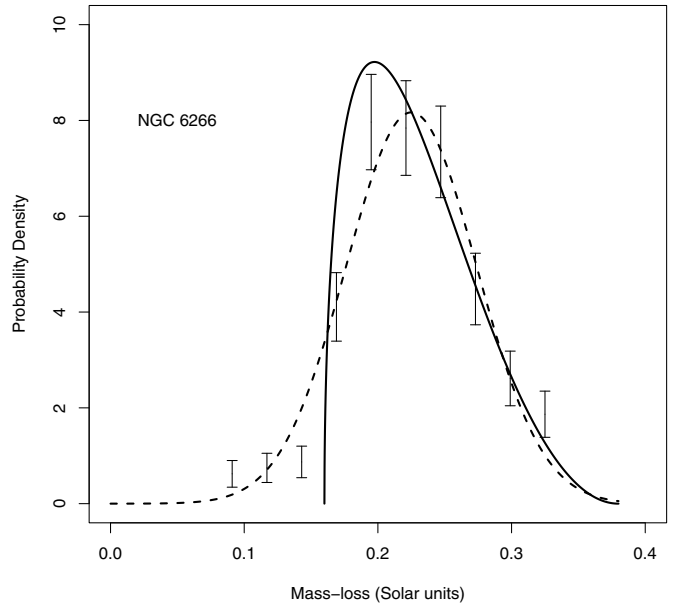

Figure 4. Mass-loss distribution in a sample of 309 HB stars in NGC 6266 from Piotto et al. (2002) *HST* data. The points represent the estimated probability density (y-axis; based on the normalized counts) for a given mass-loss bin (x-axis). The 1σ counting error is represented by the error bars. The superimposed solid black curve is our best-fit model mass-loss function. A Gaussian with the sample's mean and standard deviation is also shown as a dashed line.

of $s = 0$, as would result from a symmetric distribution, is compatible with the data in only one case (NGC 5904)[14] while the other clusters have an asymmetric distribution, as expected if our model applies. The reason why NGC 5094 has a more symmetric distribution than the other clusters, at least in the central region probed by our robust indicator of skewness, may be related to the effect of gravitational focusing, but a more in-depth analysis would be required to settle the case.

In Figure 4, we show the best-fit curve from our model superimposed onto the NGC 6266 mass-loss data, together with the Gaussian best fit. The best-fit curve (with $A = 0.222 \pm 0.007$, $B = 0.158 \pm 0.002$; we describe the fitting procedure in the Appendix) reproduces the shape of the observed mass-loss data points to a high degree of accuracy. This is evidence that in NGC 6266, stellar encounters may be able to act as the main ingredient in determining RGB mass loss. However,. However note that in Figure 4 the bins corresponding to low mass loss, below the cutoff predicted by our model, contain a small number of stars anyway. Since our model predicts strictly 0 stars there, this would result in a formal rejection of the model in statistical tests such as Pearson's χ^2 test (see below). To justify this discrepancy, stellar evolution off the ZAHB may be invoked. Evolved HB stars, i.e., stars that no longer lie on the ZAHB, may appear as higher-mass ZAHB stars because evolutionary tracks run almost parallel to the ZAHB from the blue to the red side of the CMD as stellar age increases, resulting in a contamination of the high-mass bins with lower-mass, evolved stars.

In NGC 6093, NGC 5904, and NGC 6752, the agreement between the mass-loss data and our model is somewhat less striking, but the main features (the positive skewness, left cutoff, and right long tail) are well matched, with the exception, as

_____

[14] This does not contradict the Shapiro–Wilk test result. Apparently, NGC 5094 fails the S-W test because of either asymmetry in the tails of the distribution further from the median than the first and third quartile, which are not considered by our robust skewness parameter, or due to non-zero kurtosis or issues with higher momenta.
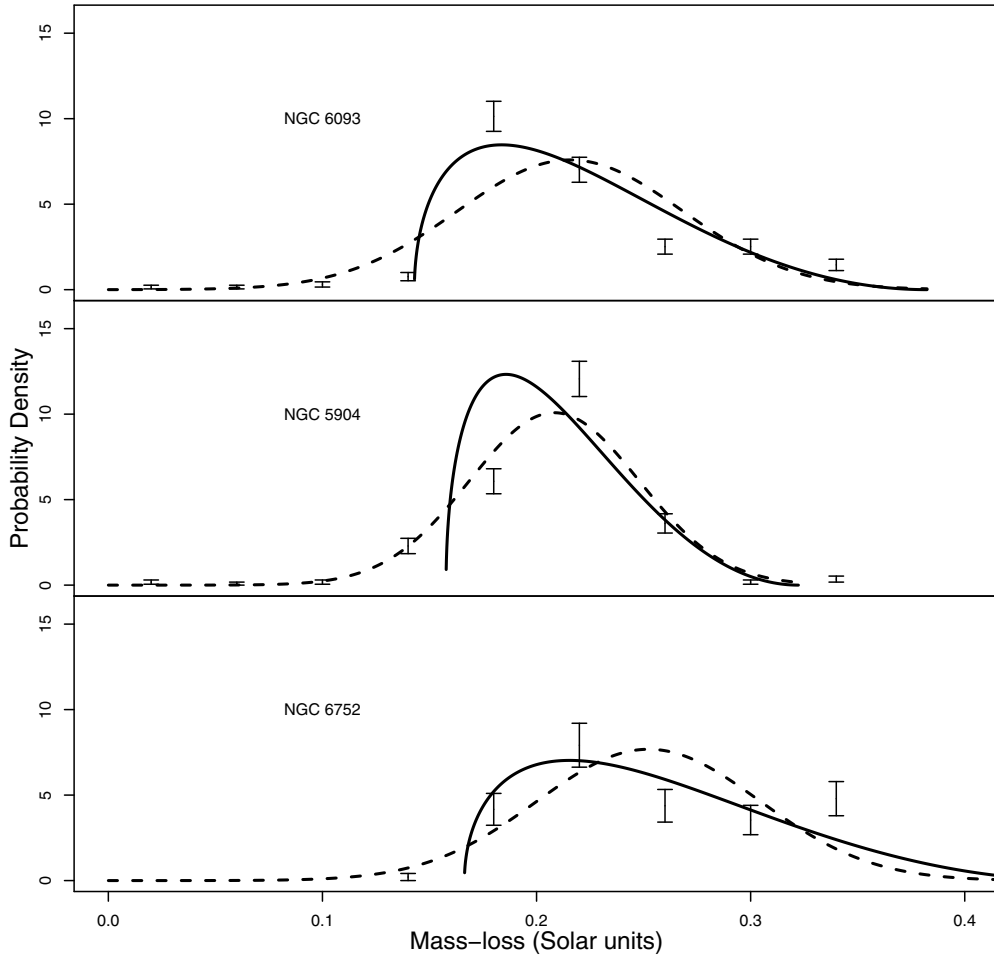
Figure 5. Best-fit models (solid lines) for mass-loss distributions of NGC 6093, NGC 5904, and NGC 6752 (points). The 1σ counting error is represented by the error bars. Gaussians with the sample's mean and standard deviation are also shown as dotted lines. Note how the Gaussian seems to miss the cutoff-like feature at the left side of the plots, but fits NGC 5904 visibly better than our model.

discussed above, of NGC 5904. We point out that this cluster has a relatively low central density with respect to the others in the sample, more than an order of magnitude less than NGC 6266 according to Harris (1996), and, as anticipated above, gravitational focusing is about three times more important in NGC 5904 compared to NGC 6266 (see ν in Table 2). On the other hand, the collision parameter $\Gamma_{\rm coll}$ is similar for the two clusters despite the differences in the shape of the mass-loss distribution. This is not surprising, given that the collision parameter determines the probability of a star colliding but does not influence the details of what happens during the collision. It is precisely those details that dictate the shape of the mass-loss distribution function. Figure 5 shows our best-fit models superimposed on the histograms of mass loss for the HB of these GCs together with the Gaussian best fit. We list in Table 3 the relevant fit parameters and uncertainties (Col 3, Col 4), and the HB star sample size (Column 2).

As a further check that our results are not unduly influenced by off-ZAHB evolution, we also compared our model to a Gaussian only in the high-mass-loss tail of the distribution, i.e., $\delta M > 0.16$. We choose this threshold because it is larger than the low-mass cutoff in all of the clusters we considered. It is also interesting to test the goodness of fit of our model in the high-mass-loss tail of the distribution (corresponding to low impact parameters in Equation (11)) because it is the least affected by environmental factors, as discussed in Section 3.1.

For each GC in our sample, we obtained mean and standard deviation estimates from the whole data set, i.e., before applying any cutoff to the mass-loss distribution. We then plugged these values into a Gaussian function and compared it to our model, whose parameters have been similarly obtained by fitting the whole data set. The comparison was carried out only on the data points above the $\delta M > 0.16$ cutoff through a Pearson's χ^2 test, i.e., by computing

$$\chi^2 = \Sigma_i \left[\frac{(N_{{\rm observed},i} - N_{{\rm predicted},i})^2}{N_{{\rm predicted},i}} \right] \quad (22)$$

over the bins above the $\delta M > 0.16$ cutoff.[15] In Table 4, we report the values of χ^2 obtained for the two distributions, i.e., either using our distribution or the Gaussian to predict the number of observations in each bin. Note that both distributions have two free parameters and are compared on the same set of data points and bins, consequently sharing the same number of degrees of freedom, which results in values of χ^2 that can be compared directly. It can be seen that in the case of NGC 5904, the Gaussian model has a lower χ^2, thus outperforming our distribution function, while in the other cases we have either

_____

[15] If we compared the models over the full range of the observations, our model would have $\chi^2 = \infty$ due to its prediction of strictly 0 points in the left tail.

Table 4
Bootstrapping Estimates of Errors on Our Model's Coefficients and χ^2 Test
Results for the High-mass-loss Tail

Name	ΔA	ΔB	Mean	S. d.	χ^2	χ^2 Gaussian	dof
NGC 5904	0.01	0.004	0.21	0.04	81.2	53.2	3
NGC 6093	0.02	0.003	0.22	0.05	37.7	95.1	3
NGC 6266	0.01	0.004	0.22	0.05	18.3	14.2	3
NGC 6752	0.02	0.006	0.25	0.05	20.5	37.9	3

Notes. Fit parameter uncertainties as estimated from a bootstrap resampling of
the mass-loss sample and refitting (ΔA, ΔB), outcome of the Pearson's χ^2 test
for our model and for a Gaussian (see text), and relevant degrees of freedom.
We also include the standard deviation and mean of the samples, that we used
as parameters for the Gaussian.

similar values (in NGC 6266) or a marked superiority of our
model (i.e., a lower value of χ^2) in NGC 6093 and 6752. In
Table 4, we also list the error bars on A and B obtained by
bootstrap resampling (with replacement) the observed mass-
loss values for each cluster, and repeating the fitting procedure
10,000 times. The associated standard deviation of the sample of
fitting parameters thus obtained is compatible with the error bars
on fit coefficients obtained through the standard linear regression
procedure as listed in Table 3.

Interestingly, Figures 4 and 5 show that RG stars need to
collisionally lose a mass as high as $\sim$0.3–0.35 $M_\odot$ in order to
account for the presence of hot HB stars. These mass-loss values
are fully compatible with the minimum total mass required for
a star to be on the hot part of the HB. Since the early '70 s,
it has been clear that a star ignites helium with a violent flash
at the RGB tip if the survived hydrogen-rich envelope mass is
a few hundredths of a solar mass over the helium core (e.g.,
Giannone et al. 1970, in the case of mass exchange in a binary
system). On the contrary, if stars undergo very high mass loss
and the hydrogen-rich envelope is reduced to a few thousandths
of a solar mass, then they leave the RGB and ignite helium
with a late flash while descending the WD cooling curve (e.g.,
Castellani & Castellani 1993; D'Cruz et al. 1996; Brown et al.
2001). Moreover, during this phase, hot HB stars can experience
a flash-induced mixing inside the helium core able to reach
the hydrogen-rich envelope (see, e.g., Cassisi et al. 2003) with
observational consequences on their surface abundances (Moni
Bidin et al. 2012). All of these previous investigations assumed
the Reimers' formalism to describe the mass-loss process by
changing the Reimers' parameter (η_R) up to 1 or more. This
can be defined as a "slow" mass-loss mechanism since the mass
loss progressively increases as stellar luminosity increases and
gravity decreases. In order to reproduce the collision picture, we
computed new evolutionary models with the stellar evolution
code ATON (Ventura et al. 2008) by applying an instantaneous
(episodic) mass stripping (δM_{coll}) to a star with an initial mass
of $M = 0.8\,M_\odot$, $Z = 0.0006$, and $Y = 0.24$. In the models, we
assumed that the collision occurs when the helium core mass is
$M_{core} \simeq 0.45 M_\odot$ and lasts nearly 100 yr, and for different values
of δM_{coll}. In Figure 6, three representative cases are shown.
After the collision event, the star reacts to the instantaneous
mass loss and attempts to rearrange the structural quantities of
its envelope according to the instantaneous total mass. When
$\Delta M_{coll} \sim 0.36\,M_\odot$ (bottom panel), the star does not succeed in
igniting helium due to the very low residual envelope mass. If
the stripped mass is slightly lower, e.g., $\delta M_{coll} \sim 0.26$, then the
star rapidly crosses the Hertzsprung–Russell diagram toward
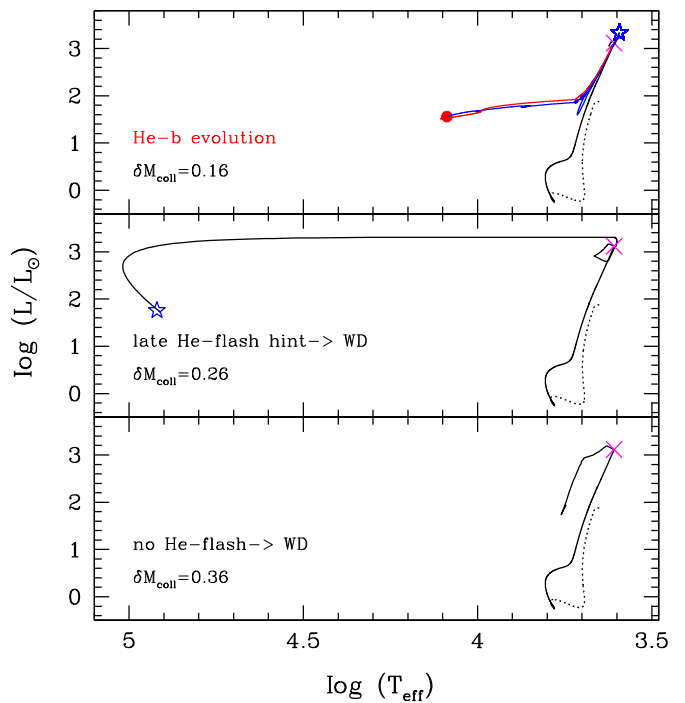high effective temperatures ($\log T_{eff} \sim 4.9$) before experiencing

Figure 6. Evolution of a star with initial mass $M = 0.8\,M_\odot$ and chemical
composition $Z = 0.0006$, $Y = 0.24$, from the pre-MS (black dotted line)
to the RGB and the subsequent phases (solid line). Three representative
cases are shown: from top to bottom, collision mass loss is $\delta M_{coll} =$
0.16, 0.26, and 0.36 $M_\odot$. In each panel the fate of star is labeled; the magenta
cross shows the RGB point where the collision mass-loss event takes place; and
the blue star indicates the first-primary He-flash occurrence. In the upper panel,
the blue line refers to the evolution toward the ZAHB model (red dot) and the
red line illustrates the off-ZAHB evolution.

(A color version of this figure is available in the online journal.)

a late helium flash. Nevertheless, the surviving hydrogen-rich
layer is so small that it is rapidly exhausted by the shell above
the helium-rich core, the helium burning switches off and the
star becomes a WD. For a collisional mass loss lower than
$\sim$0.2 $M_\odot$, the star experiences the helium flash at high or
low effective temperatures proceeding to a "normal" helium-
burning evolutionary sequence. For the aforementioned ages
and values of metal content, the RGB-tip star mass is of the
order of $0.80\,M_\odot$ and the helium-core mass at the helium-
flash is $\sim$0.5 $M_\odot$. Therefore, if after the collision the survived
envelope mass is $\gtrsim 0.05\,M_\odot$, then the subsequent evolution
does not show substantial changes after the short time needed to
rearrange all of its structural quantities. A more complete study
of this matter is beyond the scope of this paper, but we plan to
deepen this issue in a forthcoming paper.

5. CONCLUSIONS AND FUTURE PROSPECTS

We presented a simple dynamical model for enhanced mass
loss in the RGB phase through tidal stripping in stellar encoun-
ters. The model predicts a distinctively asymmetric distribution
of mass loss, with a tail toward high values of mass loss. The re-
sulting distribution function contains only two freely adjustable
parameters that regulate the overall amount and the spread in
mass loss, while the distribution shape is fixed. We checked our
model against the distribution of HB mass in four Galactic EHB
GCs from *Hubble Space Telescope* (*HST*) CMDs. Given an ini-
tial RGB-tip mass, this results in a distribution of mass loss in
the RGB phase that we compared to our model. The obtained

mass-loss distribution is skewed, except for NGC 5904, and an S-W test suggests that the distribution is not Gaussian. Our simple dynamical model of mass loss reproduces the shape of the mass-loss distribution with satisfactory to excellent accuracy, showing that stellar encounters may act as the main component in determining RGB mass loss.

Both photometric data sets that we used refer to Galactic globular clusters (GGC) core regions. In a more extended comparison between our model and observations, a difference in the stellar number ratio between EHB and red HB stars in the less collisional GC outskirts and its core might be possible, even though this will depend on star orbits and the cluster size. For a typical GC mass ($10^5 M_\odot$) and half-mass radius (3 pc), the timescale on which orbits in the cluster mix (i.e., the crossing time) is of the order of $\sim 3.5 \times 10^5$ yr, which is very much smaller than the GGC ages. Results from radial distribution studies and number ratios in the center and outskirts of GCs are still an open issue. A study of NGC 2808 by Iannicola et al. (2009) has revealed that the relative fractions of cool, hot, and extreme HB stars do not change radically when moving from the center to the outskirts of that cluster. The authors argued against the presence of strong radial differentiation among any stellar subpopulations having distinctly different helium abundances. Interestingly, the ratio of HB to RGB stars brighter than the ZAHB luminosity level steadily increases when moving from the innermost to the outermost cluster regions, which is a possible indication of a deficiency of bright RGB stars in the outskirts of the cluster. Nataf et al. (2011) showed that the HB of 47 Tuc becomes both fainter and redder for sightlines farther from the cluster center. They demonstrated that a gradient is found to be significant in the cluster outskirts, while closer in the data are more compatible with a uniform mixing. If we speculate on this feature in terms of mass loss, then heavy HB stars, i.e., those whose RG progenitors have lost a small amount of mass, are preferably located out of the center. Of course, we do not intend to correlate this observational evidence with our collision scenario, since many factors can contribute to the picture, such as differential reddening, multiple generation of stars, and different helium abundances, but rather as a hint for further study such as with photometric data obtained by new wide-field imagers (e.g., OmegaCam on the VLT Survey Telescope; Capaccioli & Schipani 2011).

In a previous paper, we showed that while HB morphology is mainly determined by metallicity, age, and helium enhancement, dynamical effects most likely are present, especially in high-density clusters suspected of undergoing core-collapse (Pasquato et al. 2013). However, the high-density environment of a collapsing core may affect RGB mass loss (and HB morphology, in turn) via various channels. Binary stars, for example, are expected to play a major dynamical role in halting core-collapse by releasing energy while becoming more bound (Hut 1983). This may result in Roche–Lobe overflow within binary systems whose primary is an RGB star and whose semiaxis shrinks enough, resulting in enhanced mass stripping (Binary Channel; Lei et al. 2013b, 2013a). On the other hand, direct stellar collisions and grazing encounters taking place on unbound orbits are also much more likely to occur when core density increases dramatically due to gravitational collapse, also resulting in enhanced mass stripping (Collisional Channel; our model presented in this paper). In this context, only a quantitative model may allow us to distinguish between the two channels. Ideally, a quantitative model should be able to predict the HB mass distribution, the rotation rate of HB stars, and their binary
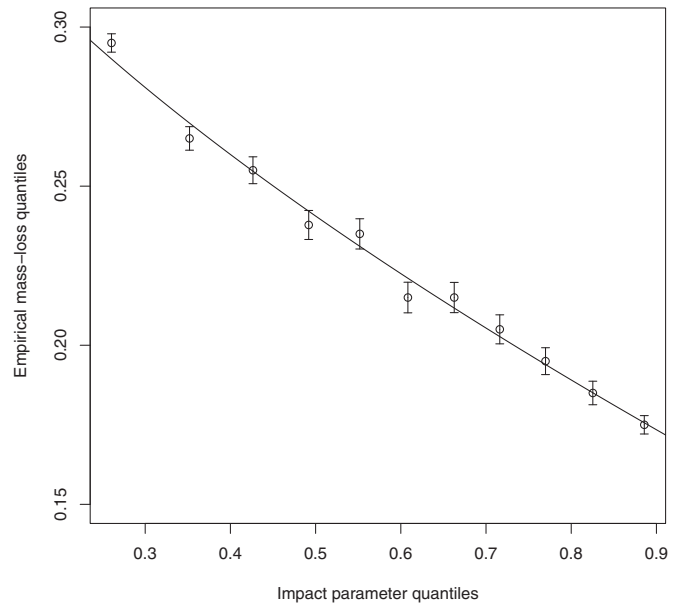

Figure 7. Empirical quantiles of mass loss for the HB stars in NGC 6266 from Piotto et al. (2002) *HST* data (*y*-axis), as a function of the corresponding theoretical quantiles of the impact parameter in a Maxwell–Boltzmann distribution (*x*-axis). The error bars are based on the uncertainty of the estimate of the quantiles for a uniform distribution function. The superimposed solid line is our best-fit model.

fraction. When the comprehensive set of SPH simulations we are running (A. Moraghan et al., in preparation) is ready, we will be able to predict both mass-loss and angular-momentum deposition, paving the way for a quantitative comparison.

APPENDIX

FITTING PROCEDURE

Equation (13) is nonlinear in the *A* and *B* parameters. It would, in principle, be possible to either use a nonlinear fitting procedure to fit it directly to the histograms of mass loss of each cluster, or to fit it "by eye." However, it is more convenient to consider Equation (10), which is linear in *A* and *B*. If for every collision that resulted in a mass loss δM_i we had the corresponding information on the impact parameter b_i, then we could directly fit Equation (10) to the sample of δM_i values as a function of b_i, using, e.g., linear least squares. Unfortunately, we do not know the b_i associated with each δM_i. However,

if we assume that the "real" $\delta M(b)$ relationship is monotonic and the b distribution is actually given by Equation (11), then the quantiles of the sample δM_i can be plotted as a function of the theoretical quantiles of the distribution in Equation (11). In Figure 7 we plot the empirical quantiles of the mass-loss sample as a function of the theoretical quantiles of b/a based on Equation (11) for NGC 6266. This, under the above mentioned hypotheses, amounts to a direct visualization of the function relating mass loss to the impact parameter, i.e., the "real" $\delta M(b)$ relationship, to which we can then fit Equation (10) using linear least squares. The values of A and B are listed in Table 3 and the associated errors are obtained in this way. This procedure is not a circular argument: the assumption that $\delta M(b)$ is monotonic and that the underlying distribution of b is actually given by Equation (11) is used only to obtain the best-fitting values of A and B, not to validate the model in the first place. Moreover, values independently obtained "by eye" directly on the histograms in Figures 5 and 4 actually closely match those listed in Table 3.

REFERENCES

Adams, T., Davies, M. B., & Sills, A. 2004, MNRAS, 348, 469
Alonso-García, J., Mateo, M., Sen, B., Banerjee, M., & von Braun, K. 2011, AJ, 141, 146
Anderson, S. B., Wolszczan, A., Kulkarni, S. R., & Prince, T. A. 1997, ApJ, 482, 870
Beccari, G., Ferraro, F. R., Possenti, A., et al. 2006, AJ, 131, 2551
Bedin, L. R., Piotto, G., Anderson, J., et al. 2004, ApJL, 605, L125
Boyer, M. L., van Loon, J. T., McDonald, I., et al. 2010, ApJL, 711, L99
Bragaglia, A., Carretta, E., Gratton, R., et al. 2010, A&A, 519, A60
Brocato, E., Castellani, V., Poli, F. M., & Raimondo, G. 2000, A&AS, 146, 91
Brown, T. M., Sweigart, A. V., Lanz, T., Landsman, W. B., & Hubeny, I. 2001, ApJ, 562, 368
Brown, T. M., Sweigart, A. V., Lanz, T., et al. 2010, ApJ, 718, 1332
Buonanno, R., Corsi, C., Bellazzini, M., Ferraro, F. R., & Pecci, F. F. 1997, AJ, 113, 706
Busso, G., Cassisi, S., Piotto, G., et al. 2007, A&A, 474, 105
Capaccioli, M., & Schipani, P. 2011, Msngr, 146, 2
Carretta, E., Bragaglia, A., Gratton, R., D'Orazi, V., & Lucatello, S. 2009, A&A, 508, 695
Carretta, E., Bragaglia, A., Gratton, R. G., Lucatello, S., & D'Orazi, V. 2012, ApJL, 750, L14
Carretta, E., Bragaglia, A., Gratton, R. G., et al. 2010, A&A, 516, A55
Cassisi, S., Schlattl, H., Salaris, M., & Weiss, A. 2003, ApJL, 582, L43
Castellani, M., & Castellani, V. 1993, ApJ, 407, 649
Catelan, M. 2009, Ap&SS, 320, 261
Dalessandro, E., Lanzoni, B., Ferraro, F. R., et al. 2008a, ApJ, 677, 1069
Dalessandro, E., Lanzoni, B., Ferraro, F. R., et al. 2008b, ApJ, 681, 311
Dalessandro, E., Salaris, M., Ferraro, F. R., Mucciarelli, A., & Cassisi, S. 2013, MNRAS, 430, 459
Dalessandro, E., Salaris, M., Ferraro, F. R., et al. 2011, MNRAS, 410, 694
D'Cruz, N. L., Dorman, B., Rood, R. T., & O'Connell, R. W. 1996, ApJ, 466, 359
Dotter, A. 2013, MmSAI, 84, 97
Dupree, A. K., Smith, G. H., & Strader, J. 2009, AJ, 138, 1485
Ferraro, F. R., Paltrinieri, B., Pecci, F. F., Rood, R. T., & Dorman, B. 1998, ApJ, 500, 311
Giannone, P., Refsdal, S., & Weigert, A. 1970, A&A, 4, 428
Gratton, R., Sneden, C., & Carretta, E. 2004, ARA&A, 42, 385
Gratton, R. G., Carretta, E., Bragaglia, A., Lucatello, S., & D'Orazi, V. 2010, A&A, 517, A81
Groenewegen, M. A. T. 2012a, A&A, 540, A32
Groenewegen, M. A. T. 2012b, A&A, 541, C3
Groenewegen, M. A. T., Sloan, G. C., Soszyński, I., & Petersen, E. A. 2009, A&A, 506, 1277
Harper, G. 1996, in ASP Conf. Ser. 109, Cool Stars, Stellar Systems, and the Sun, ed. R. Pallavicini & A. K. Dupree (San Francisco, CA: ASP), 481
Harris, W. E. 1996, AJ, 112, 1487
Heggie, D. C., & Hut, P. 1993, ApJS, 85, 347
Hills, J. G. 1975, AJ, 80, 809
Hut, P. 1983, ApJL, 272, L29
Iannicola, G., Monelli, M., Bono, G., et al. 2009, ApJL, 696, L120
Kudritzki, R. P., & Reimers, D. 1978, A&A, 70, 227
Lafon, J.-P. J., & Berruyer, N. 1991, A&ARv, 2, 249
Lee, Y.-W., Demarque, P., & Zinn, R. 1994, ApJ, 423, 248
Lee, Y.-W., Gim, H. B., & Casetti-Dinescu, D. I. 2007, ApJL, 661, L49
Lee, Y.-W., Joo, S.-J., Han, S.-I., et al. 2005, ApJL, 621, L57
Lei, Z., Zhang, F., Ge, H., & Han, Z. 2013a, arXiv e-prints
Lei, Z.-X., Chen, X.-F., Zhang, F.-H., & Han, Z. 2013b, A&A, 549, A145
Marín-Franch, A., Aparicio, A., Piotto, G., et al. 2009, ApJ, 694, 1498
McDonald, I., van Loon, J. T., Decin, L., et al. 2009, MNRAS, 394, 831
McLaughlin, D. E., & van der Marel, R. P. 2005, ApJS, 161, 304
Milone, A. P., Piotto, G., Bedin, L. R., et al. 2012, A&A, 540, A16
Monelli, M., Milone, A. P., Stetson, P. B., et al. 2013, MNRAS, 431, 2126
Moni Bidin, C., Moehler, S., Piotto, G., Momany, Y., & Recio-Blanco, A. 2009, A&A, 498, 737
Moni Bidin, C., Moehler, S., Piotto, G., et al. 2006, A&A, 451, 499
Moni Bidin, C., Villanova, S., Piotto, G., & Momany, Y. 2011, A&A, 528, A127
Moni Bidin, C., Villanova, S., Piotto, G., et al. 2012, A&A, 547, A109
Nataf, D. M., Gould, A., Pinsonneault, M. H., & Stetson, P. B. 2011, ApJ, 736, 94
Olofsson, H. 2008, Ap&SS, 313, 201
Origlia, L., Ferraro, F. R., Fabbri, S., et al. 2014, A&A, 564, A136
Origlia, L., Ferraro, F. R., Fusi Pecci, F., & Rood, R. T. 2002, ApJ, 571, 458
Origlia, L., Rood, R. T., Fabbri, S., et al. 2007, ApJL, 667, L85
Origlia, L., Rood, R. T., Fabbri, S., et al. 2010, ApJ, 718, 522
Pasquato, M., Raimondo, G., Brocato, E., et al. 2013, A&A, 554, 129
Pietrinferni, A., Cassisi, S., Salaris, M., & Castelli, F. 2006, ApJ, 642, 797
Piotto, G., King, I. R., Djorgovski, S. G., et al. 2002, A&A, 391, 945
Piotto, G., Villanova, S., Bedin, L. R., et al. 2005, ApJ, 621, 777
Piotto, G., Zoccali, M., King, I. R., et al. 1999, AJ, 118, 1727
Portegies Zwart, S. F. 1996, in IAU Symp. 174, Dynamical Evolution of Star Clusters: Confrontation of Theory and Observations, ed. P. Hut & J. Makino (Cambridge: Cambridge Univ. Press), 355
Raimondo, G. 2009, ApJ, 700, 1247
Raimondo, G., Brocato, E., Cantiello, M., & Capaccioli, M. 2005, AJ, 130, 2625
Raimondo, G., Castellani, V., Cassisi, S., Brocato, E., & Piotto, G. 2002, ApJ, 569, 975
Recio-Blanco, A., Aparicio, A., Piotto, G., de Angeli, F., & Djorgovski, S. G. 2006, A&A, 452, 875
Recio-Blanco, A., Piotto, G., de Angeli, F., et al. 2005, A&A, 432, 851
Renzini, A., & Voli, M. 1981, A&A, 94, 175
Rood, R. T. 1973, ApJ, 184, 815
Royston, J. P. 1982, Journal of the Royal Statistical Society, Series C (Applied Statistics), 31, 176
Sarajedini, A., Bedin, L. R., Chaboyer, B., et al. 2007, AJ, 133, 1658
Shara, M. M., Drissen, L., Rich, R. M., et al. 1998, ApJ, 495, 796
Ventura, P., D'Antona, F., & Mazzitelli, I. 2008, Ap&SS, 316, 93
Whitney, J. H., Rood, R. T., O'Connell, R. W., et al. 1998, ApJ, 495, 284
Yong, D., Grundahl, F., Nissen, P. E., Jensen, H. R., & Lambert, D. L. 2005, A&A, 438, 875